Branching ratios for the dissociative decay of triplet H_2

J. M. Schins, L. D. A. Siebbeles, J. Los, and W. J. van der Zande
FOM—Institute for Atomic and Molecular Physics, Kruislaan 407, 1098 SJ Amsterdam, The Netherlands

J. Rychlewski
A. Mickiewicz University, Ul. Grunwaldzka 6, 60-780 Poznan, Poland

H. Koch
Argonne National Laboratory, 9700 S. Cass Avenue, Argonne, Illinois
(Received 20 February 1991)

A systematic study has been performed on the singly excited $n=3$ triplet gerade states of molecular hydrogen using fast-neutral-beam photofragment spectroscopy. These states fluoresce to the triplet $2p$ states and are analyzed according to the energy released in the subsequent dissociation process. The resulting spectra are compared with theoretical results obtained by solving the coupled nuclear Schrödinger equation. Good overall agreement is reported for both the shape of the spectra and the branching ratios for fluorescence to either one of the triplet $2p$ states. Rotational and vibrational couplings that affect the $n=3$ triplet gerade complex are well described by theory.

PACS number(s): 33.70.Ca, 33.80.Gj

I. INTRODUCTION

In the preceding paper (hereafter called paper I) a description of the hydrogen $n=3$ triplet gerade complex is given that takes into account rotational and vibrational perturbations [1]. In light of these calculations, reassignments in the hydrogen $h\,^3\Sigma_g^+$ state $v=2$ and 3 series have been proposed. Similar nonadiabatic calculations by Senn, Quadrelli, and Dressler on the $n=2,3$ singlet ungerade complex are already known [2]. The triplet complex under study, which consists of the $g\,^3\Sigma_g^+$, $h\,^3\Sigma_g^+$, $i\,^3\Pi_g$, and $j\,^3\Delta_g$ states, differs from the singlet complex in the degree of mixing in the nonadiabatic states. While Senn, Quadrelli, and Dressler calculate mixing coefficients of a few percent leading to energy corrections with respect to the adiabatic energy levels of a few wave numbers, the triplet complex confronts one with mixing coefficients through practically the whole range (0–80%) leading to nonadiabatic energy corrections up to a few hundred wave numbers. These energy corrections are so large, especially for the $^3\Sigma_g^+$ states, that the connection of adiabatic energy levels to the observed levels loses all relevance. In the past this caused a confusion in nomenclature. As proposed in paper I, in the present contribution we call the third adiabatic (theoretical) $^3\Sigma_g^+$ state *and* the $3d$-like nonadiabatic (observed) state $g(3d)\,^3\Sigma_g^+$; we call the second adiabatic (theoretical) $^3\Sigma_g^+$ state *and* the $3s$-like nonadiabatic (observed) state $h(3s)\,^3\Sigma_g^+$.

A very sensitive probe of the degree of mixing in the $n=3$ triplet gerade states is the branching ratio for fluorescence to the $b(2p\sigma)\,^3\Sigma_u^+$ and $c(2p\pi)\,^3\Pi_u$ states. In this respect the present paper is a sequel to earlier work by Koot *et al.* [3] and contributes to the $n=3$ triplet gerade complex discussion by presenting a systematic set of experimental data laying bare the electronic structure of the heavily perturbed states. We discuss in detail the nature of the electronic mixing in the nonadiabatic states and its consequences for fluorescence branching ratios to the two lower ungerade $2p$ states.

II. EXPERIMENT

Since the apparatus has been described in detail before [4], we will limit ourselves to a brief discussion. A schematic drawing is shown in Fig. 1. Hydrogen molecular ions are formed in a colutron plasma source, accelerated to an energy $E_0=5500$ eV, mass analyzed, and finally charge exchanged on cesium vapor. The remaining ions are bent away from the beam by a static electric field. Fragments from short-lived molecular states scatter out of the beam and are removed by a diaphragm. In this way a neutral hydrogen beam is obtained in the metastable $c\,^3\Pi_u^-$ state (lifetimes in the order of a millisecond for the lower rovibrational levels). Rovibrational levels in the $n=3$ triplet complex are selectively excited with a dye laser and dissociate after photon emission to the $2p$ states. After a flight length of 79 cm, the fragments are detected with a position- and time-sensitive detector [5]. Intact molecules are intercepted by a beam flag to reduce the background signal from metastable decay and collision-induced dissociations. The kinetic energy released in the dissociation process is deduced from the fragment positions with short time differences ($\tau<2$ ns corresponding to dissociation angles around 90°).

For the lower vibrational and rotational levels the selectively excited $n=3$ triplet states can only decay via photon emission to either one of the $c(2p\pi)\,^3\Pi_u$, the $b(2p\sigma)\,^3\Sigma_u^+$, or the $e(3p\sigma)\,^3\Sigma_u^+$ states. Emission to the higher-lying $e\,^3\Sigma_u^+$ state cannot be observed with our apparatus. This transition is expected to be about 1000 times weaker than emission to the $b\,^3\Sigma_u^+$ state since spontaneous fluorescence scales with the third power of pho-

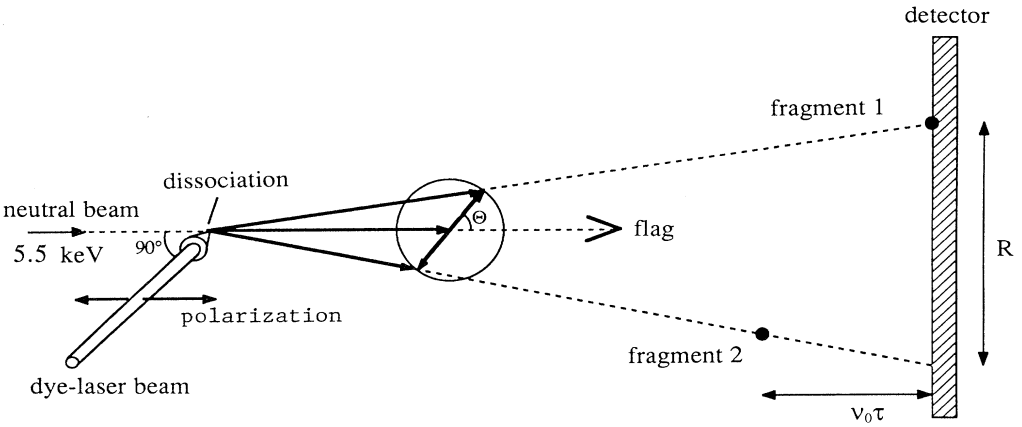

FIG. 1. Schematic experimental setup. The kinetic energy released in the dissociation process of the hydrogen molecule into two atoms is determined as $\varepsilon/E_0=(R/2L)^2$, with beam energy $E_0=5500$ eV, and flight length $L=790$ cm.

ton energy. Fluorescence to the $e\,^3\Sigma_u^+$ state does not influence the branching results presented in this paper in any case. Emission to the metastable negative-parity component of the $c\,^3\Pi_u$ state cannot be detected in our apparatus either. The positive component predissociates by rotational coupling with the $b\,^3\Sigma_u^+$ state and can be observed. The energy spectra that are recorded arise from dissociative processes that occur after fluorescence to both positive-parity $2p$ singly excited triplet states, the predissociated $c\,^3\Pi_u^+$ state, and the directly dissociative $b\,^3\Sigma_u^+$ state. Figure 2 illustrates the relation between the nuclear vibrational wave function in the excited state and the resulting kinetic-energy-release (KER) spectrum. For

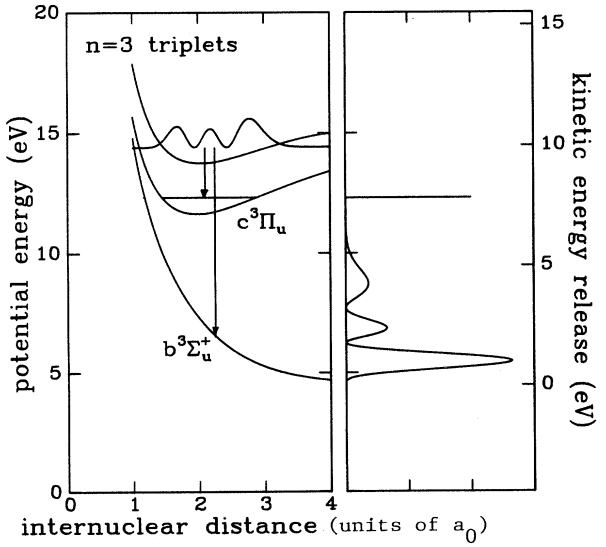

FIG. 2. Potential-energy diagram showing some relevant triplet states in hydrogen (leftmost box). Zero energy is defined as the ground-state level of hydrogen. The box at the right shows the resulting kinetic-energy-release (KER) spectrum and is therefore zeroed at the $b\,^3\Sigma_u^+$ state dissociation limit (twice the ground-state atomic hydrogen formation energy). Fluorescence from the excited state to the $b\,^3\Sigma_u^+$ state gives rise to the undulating KER spectrum, and photon emission to the $c\,^3\Pi_u^+$ state causes a sharp rotational predissociation peak.

every dissociation the sum of photon energy and KER is a constant, namely, the difference between the excited-state energy and the $b\,^3\Sigma_u^+$ state dissociation limit $H(1s)+H(1s)$ energy. The fluorescence spectrum to the $b\,^3\Sigma_u^+$ state ranges from visible to far UV, and corresponds to a KER spectrum ranging from 0 to 7 eV. Around 8 eV a peak due to predissociation of the $c\,^3\Pi_u^+$ state appears (Fig. 2). In experimental energy spectra, which will be discussed below, this peak appears broadened with a tail towards lower energy. The reason for this tail is the finite radiative lifetime (about 20 ns) of the excited-state rovibrational levels [3]: In our beam experiment this finite lifetime yields apparent lower kinetic release energies due to dissociation downstream with respect to the laser interaction region (see Fig. 1). A combination of this lifetime broadening and intrinsic detector resolution prevents distinction between *P*- and *R*-branch fluorescence decay.

III. THEORY

In the following the symbols i and f indicate initial and final states, respectively. For details of the algebra underlying the present calculations we refer to paper I and to Koot *et al.* [3]. With respect to the latter work two improvements have been made. We used *ab initio* calculated transition dipole moments and did not approximate the excited-state vibrational wave functions.

The golden-rule formula gives the transition rate T_{if} for fluorescence from the initial excited $n=3$ states to the final $2p$ states in terms of the transition dipole matrix element $\underline{M}_{if}$ (atomic units are used throughout):

$$T_{if}=\frac{32\pi^3\nu^3}{3c^3}|\underline{M}_{if}|^2\,, \tag{1}$$

$$\underline{M}_{if}=\langle i|e\mathbf{r}|f\rangle\,, \tag{2}$$

where the integral represented by brackets has to be performed over all coordinates: electronic ($\mathbf{r}$), nuclear vibrational (R), and rotational (ϕ,θ), and ν stands for the

fluorescence frequency. The spin-excluded initial-state total wave function $\Psi_i(\mathbf{r},\mathbf{R})$ is expanded in a basis of electronic-rotational functions $\psi_k(\mathbf{r},\mathbf{R})$:

$$\Psi_i(\mathbf{r},\mathbf{R})=\sum_{k=1}^{6}\frac{1}{R}\psi_k(\mathbf{r},\mathbf{R})f_k(R)\ . \tag{3}$$

The expansion is reduced to the six states that form the $n=3$ triplet gerade complex ($g\,^3\Sigma_g^+$, $h\,^3\Sigma_g^+$, $i\,^3\Pi_g^{\pm}$, and $j\,^3\Delta_g^{\pm}$). We modified the two $^3\Sigma_g^+$ states into new, diabatic states, which we call the $s(3s)\ ^3\Sigma_g^+$ and $d(3d)\ ^3\Sigma_g^+$ states. Detailed arguments for this basis-set transformation can be found in paper I. The expansion coefficients $f_k(R)$ in the above equation depend on internuclear separation. In the case of a one-state approximation (in which the expansion reduces to a single term) the expansion coefficient $f_k(R)$ is identical to the vibrational wave function. However, due to the strong vibrational and rotational coupling that affects the $n=3$ triplet gerade complex, all six states need to be considered.

The bracket integrals of Eq. (2) over electronic and rotational coordinates can be done analytically and yield a transition dipole moment $\mu_{kf}(R)$ and a $3j$ symbol, respectively; the integral over the internuclear distance that remains reads

$$\underline{M}_{if}=\int_0^{\infty}dR\ \chi_f(R)\times\sum_{k=1}^{6}\begin{pmatrix}N_f & 1 & N_k\\ -\Lambda_f & \Lambda_f-\Lambda_k & \Lambda_k\end{pmatrix}\mu_{kf}(R)f_k(R)\ . \tag{4}$$

$\chi_f(R)$ represents the vibrational wave function of the final state; N and Λ are the absolute magnitude of the total (spin-excluded) angular momentum and its projection on the molecular axis, respectively.

In Eq. (1) all quantum numbers of both initial and final states are well defined. In order to calculate transition rates that can be compared to the observations, the transition rate has to be summed over the initial-state magnetic quantum number M, as well as over the final-state quantum numbers N' and M'. Siebbeles *et al.* showed the isotropic character of the $c\,^3\Pi_u$ state as prepared by charge exchange on cesium [6], and we can assume all $c\,^3\Pi_u$ state magnetic sublevels to be equally populated.

We define the branching ratio R_i as the total fluorescence transition rate from the initial excited state to the $c(2p\pi)\ ^3\Pi_u^+$ state divided by that to the $b(2p\sigma)\ ^3\Sigma_u^+$ state. After summation over the magnetic sublevels it reads

$$R_i=\frac{\sum_{N_c}'(2N_c+1)\nu_{ic}^3|\underline{M}|_{ic}|^2}{\sum_{N_b}'(2N_b+1)\int_0^{\infty}d\varepsilon\,\nu_{\varepsilon}^3|\underline{M}_{ib}|^2} \tag{5}$$

with ν_ε the energy-dependent fluorescence frequency to the $b\,^3\Sigma_u^+$ state and ν_{ic} the fluorescence frequency to the $c\,^3\Pi_u^+$ state. The accent accompanying the summation symbols is a short-hand notation indicating that the familiar selection rules for electric dipole transitions must be satisfied [7]. The nuclear vibrational wave functions $\chi_f(R)$ of the $2p$ states are solutions to the one-state heavy-particle Schrödinger equation and were calculated using the standard Numerov algorithm; the amplitudes $f_k(R)$ describing the vibrational motion of the excited states were taken from paper I; the adiabatic *ab initio* transition dipole moments are given in Table I. The transition dipole matrix elements [Eq. (4)] and the branching ratios [Eq. (5)] are now determined without the use of adjustable parameters.

IV. RESULTS AND DISCUSSION

A. $b\,^3\Sigma_u^+$ state KER spectra

In the case of fluorescence to the $b\,^3\Sigma_u^+$ state the transition dipole matrix element [Eq. (4)] depends on the continuum wave-function (final-state) energy. It can directly be used to calculate the shape of the KER spectrum:

$$I_{ib}(\varepsilon)=\nu_\varepsilon^3|\underline{M}_{ib}(\varepsilon)|^2\ . \tag{6}$$

Figures 3(a) and 3(b) show KER spectra resulting from

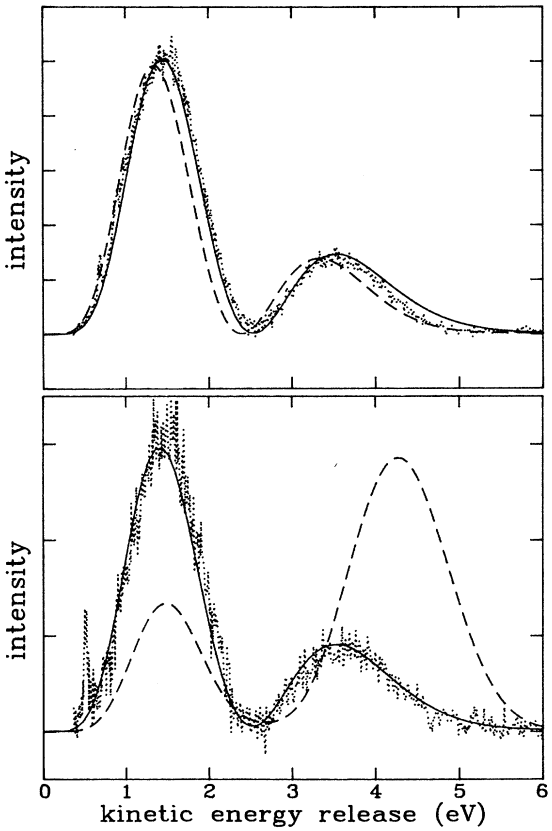

FIG. 3. Kinetic-energy-release spectra resulting from decay of $n=3$ triplet gerade states after fluorescence to the $b\,^3\Sigma_u^+$ state. The dashed and solid curves represent adiabatic (one-state) and nonadiabatic (six-state) calculations, respectively. The experimental spectrum is represented by solid circles. (a) shows the $g\,^3\Sigma_g^+$ state, $v=1$, $N=1$; (b) shows the $h\,^3\Sigma_g^+$ state, $v=1$, $N=1$. A peak appearing near 0.5 eV is due to a $j\,^3\Delta_g$ state resonance and is not discussed in the text.

TABLE I. Adiabatic transition dipole moments in atomic units for the singly excited $3s,3d$-$2p$ transitions in molecular hydrogen.

	$b(2p\sigma)\ ^3\Sigma_u^+$			$c(2p\pi)\ ^3\Pi_u$			
R (a.u.)	$g(3s\sigma)$[a]	$h(3d\sigma)$[a]	$i(3d\pi)$[b]	$g(3s\sigma)$[a]	$h(3d\sigma)$[a]	$i(3d\pi)$[c]	$j(3d\delta)$[c]
1.00	0.120 66	1.364 87		0.760 35	−1.044 56		
1.10				0.722 24	−1.046 27		
1.20	−0.092 43	1.114 90		0.688 70			
1.30				0.660 40	−1.051 22	1.800	−1.999
1.40	−0.234 96	0.902 81	0.7853	0.638 09	−1.053 54	1.807	−2.000
1.50	−0.288 19	0.814 22	0.7108	0.624 49	−1.054 37	1.815	−2.003
1.60	−0.326 57	0.734 72	0.6480	0.624 17	−1.050 95	1.825	−2.007
1.70	−0.369 96	0.659 24	0.5958	0.648 39	−1.036 00	1.836	−2.013
1.80	−0.433 89	0.570 18	0.5527	0.730 80	−0.983 02	1.848	−2.019
1.90	−0.563 90	0.387 92		0.978 62	−0.764 38	1.861	−2.027
1.95	−0.636 35	0.211 07		1.135 95	−0.482 16		
2.00	−0.656 18	0.044 17	0.4907	1.220 33	−0.206 12		
2.05	−0.643 96	−0.057 05		1.241 56	−0.035 26		
2.10	−0.626 39	−0.113 39	0.4698	1.245 80	0.059 09	1.888	−2.045
2.20	−0.597 17	−0.167 03	0.4535		0.145 84	1.903	−2.056
2.30	−0.577 31	−0.189 46	0.4416	1.260 24	0.179 21	1.919	−2.067
2.40	−0.564 46	−0.199 58	0.4336			1.935	−2.079
2.50	−0.556 97	−0.203 25	0.4299	1.291 09	0.195 82	1.951	−2.092
2.60	−0.553 81	−0.204 83	0.4285	1.310 37	0.194 70	1.966	−2.105
2.70	−0.554 34	−0.203 99	0.4306			1.980	−2.118
2.80	−0.557 97	−0.202 16	0.4353			1.992	−2.132
2.90	−0.563 26	−0.199 64	0.4414		0.180 35	2.003	−2.146
3.00	−0.573 47	−0.196 72	0.4510	1.403 37	0.174 33	2.010	−2.160
3.10			0.4644		0.168 55	2.015	−2.174
3.20			0.4810			2.014	−2.188
3.30			0.5011		0.156 16	2.008	−2.202
3.40			0.5250			1.995	−2.215
3.50	−0.647 95	−0.180 26	0.5530	1.539 16	0.147 65	1.973	−2.229
3.60			0.5855			1.939	−2.241
3.70			0.6216		0.139 90	1.892	−2.254
3.80					0.136 93	1.828	−2.266
3.90						1.746	−2.277
4.00	−0.746 84	−0.162 78		1.677 34	0.133 20	1.643	−2.288
4.10						1.522	−2.298
4.20						1.385	−2.308
4.30						1.238	−2.316
4.40						1.087	−2.325
4.50						0.941	−2.332
4.60						0.804	−2.338
4.70						0.679	−2.344
4.80						0.567	−2.350
4.90						0.469	−2.354
5.00	−0.880 00	−0.105 40		1.905 82	0.146 06	0.384	−2.358
5.10						0.311	−2.361
5.20						0.249	−2.363
5.30						0.196	−2.365

decay of the $v=1, N=1$ levels of the g and $h\ ^3\Sigma_g^+$ states after background subtraction. The dashed and solid curves show the results of adiabatic (one-state) and nonadiabatic (six-state) calculations, respectively.

The experimental spectra look very similar to one another. The decrease in intensity as a function of KER reflects the ν^3 factor in emission of Eq. (6). The node in the spectrum reflects the vibrational $v=1$ character of the selectively excited states. A difference between the spectra is the signal-to-noise ratio: The $g\ ^3\Sigma_g^+$ state transitions are much stronger than those of the $h\ ^3\Sigma_g^+$ state. The reason is that the $g\ ^3\Sigma_g^+$ state, being of dominant $3d$ character, has a much stronger electronic transition dipole to the $b\ ^3\Sigma_u^+$ state (of $2p$ character) than the $3s$-like $h\ ^3\Sigma_g^+$ state. A similar situation occurs in the atomic limits, where $3d$-$2p$ transitions are stronger than the $3s$-$2p$ transitions. Apart from signal intensity these two spectra can hardly be distinguished. They both display a regular, double maximum shape, as can be expected for transitions originating from a harmoniclike excited-state electronic potential. Indeed, both $^3\Sigma_g^+$ state potential-energy curves are nearly identical: In Fig. 2 they would be, for

TABLE I. (*Continued*).

	$b(2p\sigma)\ ^3\Sigma_u^+$			$c(2p\pi)\ ^3\Pi_u$			
R (a.u.)	$g(3s\sigma)$[a]	$h(3d\sigma)$[a]	$i(3d\pi)$[b]	$g(3s\sigma)$[a]	$h(3d\sigma)$[a]	$i(3d\pi)$[c]	$j(3d\delta)$[c]
5.40						0.151	−2.367
5.50						0.112	−2.367
5.60						0.080	−2.368
5.70						0.054	−2.368
5.80						0.032	−2.368
5.90						0.013	−2.368
6.00				2.119 91	0.467 43	0.002	−2.368
6.10						0.014	−2.367
6.20						0.024	−2.367
6.30						0.031	−2.366
7.00				2.231 55	0.744 87		
8.00				2.342 23	0.886 30		

[a]J. Rychlewski, Ref. [11].
[b]H. Koch, Ref. [12].
[c]H. Koch, Ref. [13].

small internuclear separation, indistinguishable.

The adiabatic calculations [dashed curves in Figs. 3(a) and 3(b)] do not represent the experimental data satisfactorily. For the $g\ ^3\Sigma_g^+$ state the energy of the zeros is shifted. The failure to reproduce the amplitude of the $h\ ^3\Sigma_g^+$ state is due to the sudden change in the adiabatic transition dipole moment (Table I). Similar discrepancies are found for all measured $^3\Sigma_g^+$ state rovibrational levels. In a previous publication the $h\ ^3\Sigma_g^+$ state discrepancy was shown to originate from the electronic character exchange of the $^3\Sigma_g^+$ states around equilibrium internuclear separation [8]. This electronic character exchange can be most clearly appreciated from the $g\ ^3\Sigma_g^+$ state adiabatic transition dipole moment, which has a node near equilibrium internuclear separation (see Table I). This change in electronic character of the adiabatic states and the strong mixing in the nonadiabatic states makes a connection between adiabatic and nonadiabatic $^3\Sigma_g^+$ states hardly possible and irrelevant. In the present comparison of adiabatic theory with experiment we chose to associate the adiabatic $g\ ^3\Sigma_g^+$ state with the weakly radiating nonadiabatic $h\ ^3\Sigma_g^+$ state. As explained in detail in paper I, the connection between nonadiabatic and electronic $^3\Sigma_g^+$ states is straightforward in a diabatic electronic basis set. The nonadiabatic $g\ ^3\Sigma_g^+$ state then mainly consists of the diabatic electronic $3d\ ^3\Sigma_g^+$ state, and the nonadiabatic $h\ ^3\Sigma_g^+$ state mainly of the diabatic electronic $3s\ ^3\Sigma_g^+$ state. The solid curves in Figs. 3(a) and 3(b) represent results of nonadiabatic calculations and represent the experimental data very well in both cases. The electronic basis transformation is used to transform adiabatic to diabatic transition dipole moments. Figures 4(a) and 4(b) display the diabatic transition dipole moments to the $b\ ^3\Sigma_u^+$ and $c\ ^3\Pi_u$ states, respectively. The $g\ ^3\Sigma_g^+$ state node has disappeared. The remaining R dependence is comparable in magnitude to that of the $i\ ^3\Pi_g$ and $j\ ^3\Delta_g$ state transition dipole moments. Note that the $j\ ^3\Delta_g$ to $b\ ^3\Sigma_u^+$ state transition dipole moment is not given. It vanishes identically according to the electric dipole selection rule $\Delta\Lambda=0,\pm1$. Due to this selection rule, the $j\ ^3\Delta_g^-$ state spectra result from the electronic $i\ ^3\Pi_g$ state potential exclusively, as was already pointed out by Koot *et al.* [3]. Even if the nonadiabatic $j\ ^3\Delta_g^-$ state consists of mainly

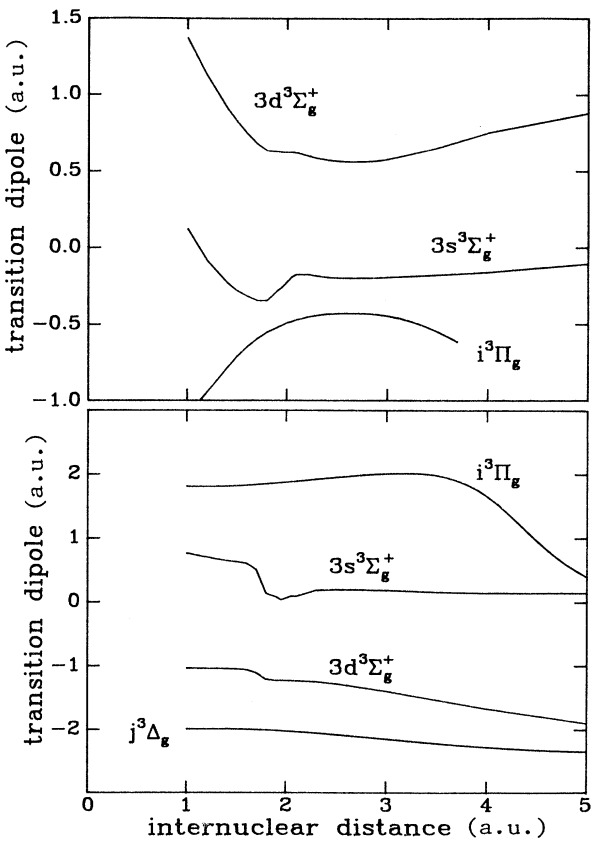

FIG. 4. Plot of the diabatic transition dipole moments calculated from the adiabatic data presented in Table I. (a) shows the $n=3$ triplet gerade to $b\ ^3\Sigma_u^+$ state transitions; (b) shows the $n=3$ triplet gerade to $c\ ^3\Pi_u$ state transitions.

electronic $j\,^3\Delta_g$ state character, radiation to the $b\,^3\Sigma_u^+$ state can only be observed insofar as an electronic $i\,^3\Pi_g$ state component is available.

The shape of a KER spectrum immediately reveals the vibrational quantum number of the excited state. In the one-state approximation the dissociative $b\,^3\Sigma_u^+$ state can be thought of as a mirror mapping the vibrational probability distribution onto the KER scale (see Fig. 2). Indeed, Koot *et al.* have shown the stationary phase approximation to apply rather well: In this approximation the overlap between the excited state and continuum vibrational wave functions is determined by a small region in the internuclear distance domain, which justifies the association of small internuclear distance domains with (mirrored) small KER domains [3]. The full quantum-mechanical expression [Eqs. (4) and (6)] does not allow for such a correspondence.

In the nonadiabatic case, in which more than one electronic state is involved, this semi-classical node correspondence in KER and internuclear distance domains is lost. Spectra from negative-parity excited states show zeros as in the one-state approximation, but the vibrational probability distribution $P(R) = \int d\mathbf{r}\, d\Omega |\Psi(\mathbf{r},\Omega,R)^2 = \sum_{k=1}^{6} |f_k(R)|^2$ does not vanish at some R value, in general.

B. Branching ratios

For many rovibrational levels in the $n=3$ triplet gerade complex we recorded KER spectra. From them we extracted the experimental branching ratios by simply dividing the number of counts of the $c\,^3\Pi_u^+$ state structure by that of the $b\,^3\Sigma_u^+$ state structure. These ratios are presented in Fig. 5 as a function of angular momentum N. As one can see, the trends are very well reproduced by theory. Apart from the $v=0$ series of the $g\,^3\Sigma_g^+$ state we can even report good quantitative agreement. The use of a hot plasma ion source permitted acquisition of spectra for angular momenta up to $N=7$.

The experimental error has two main sources. The first one is the signal-to-noise ratio. As the $b\,^3\Sigma_u^+$ state structure is extended over a range of 7 eV, and the $c\,^3\Pi_u$ state predissociation peaks extend over less than 0.5 eV, the error bars become important for $R_i > 1$. A second source of error is given by the background subtraction procedure uncertainty. The spectra as displayed in Figs. 3(a) and 3(b) result after subtraction of a background due to decay of states other than the resonantly excited one, either with or without previous photon absorption. Background subtraction is simplified by the presence of minima in the spectrum. In practice this means that the

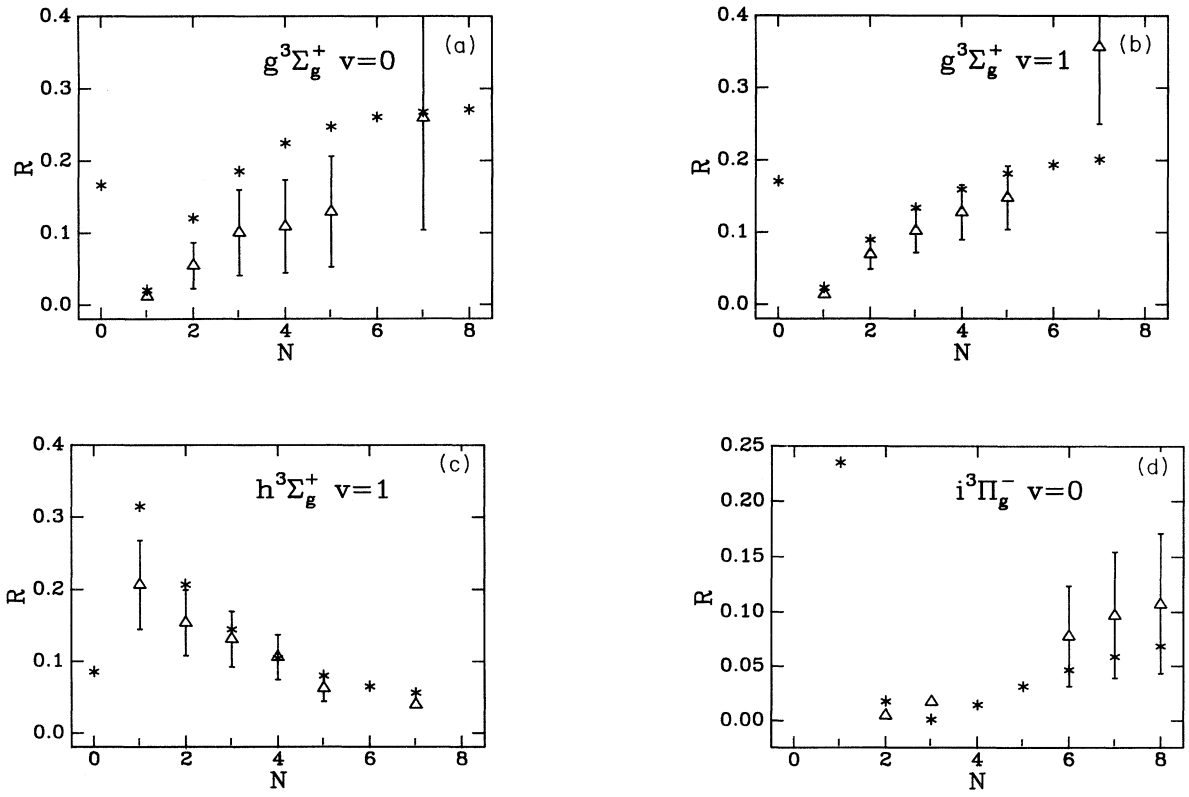

FIG. 5. Branching ratios $R = I_c/I_b$ for fluorescence decay of the $n=3$ triplet gerade states to the $b(2p\sigma)\ ^3\Sigma_u^+$ and $c(2p\pi)\ ^3\Pi_u^+$ states as a function of angular momentum N. Stars mark the nonadiabatic theoretical data; triangles with error bars represent experimental data.

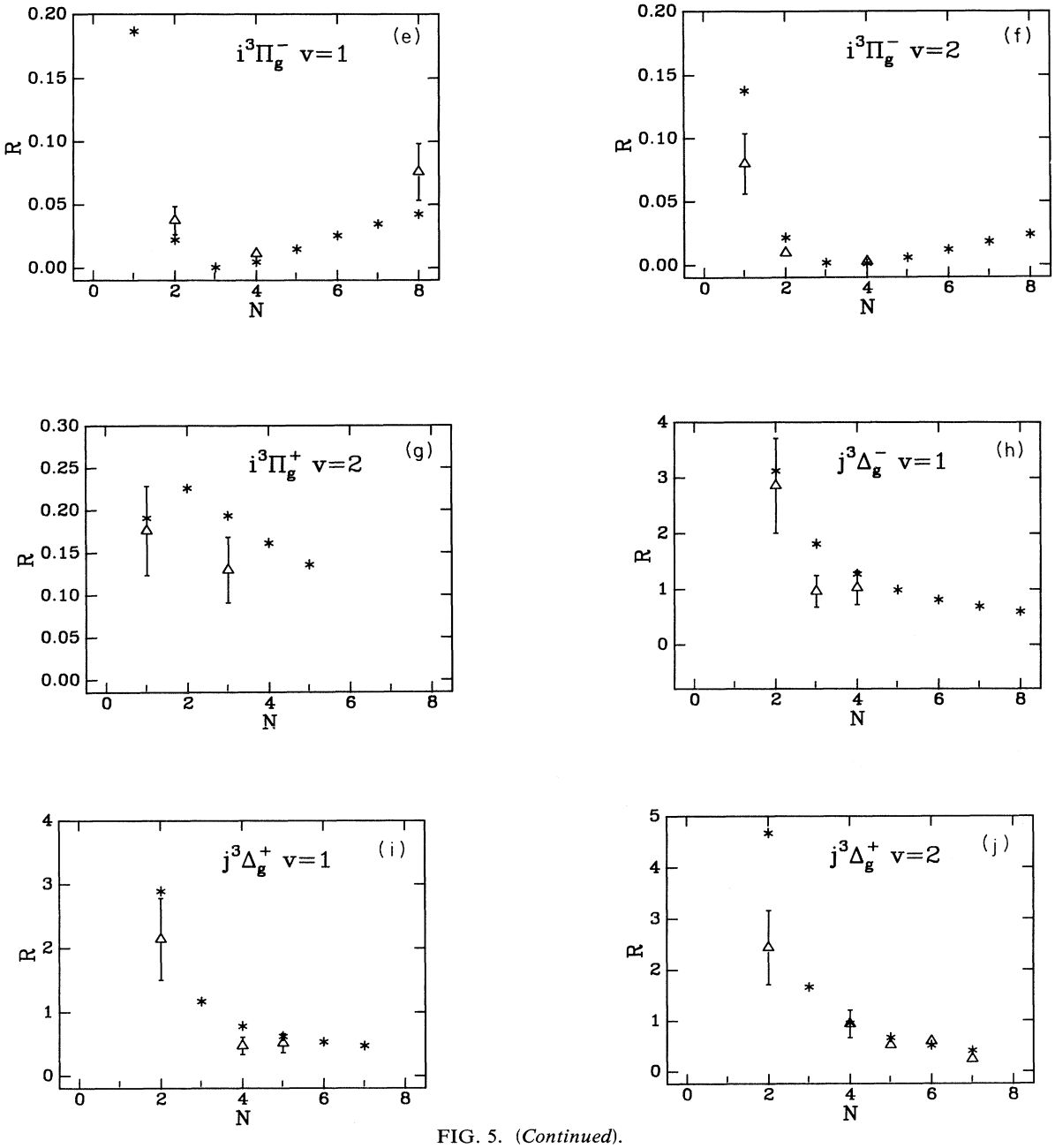

FIG. 5. (*Continued*).

error bars for the $v=0$ series are significantly larger than the others. A third error is caused by the difference in anisotropy for radiative decay to either one of the $2p$ states. The $b\ ^3\Sigma_u^+$ state is repulsive and the $c\ ^3\Pi_u^+$ state is predissociated rotationally. From the angular spectra we indeed observed a very small difference in anisotropy, but it leads to significantly smaller errors than the former two, and this source of error is not included.

The branching ratios show a complicated behavior. In the following we explain this behavior in terms of the excited-state mixing, as manifested by the expansion coefficients $f_i(R)$ of Eq. (3).

1. $^3\Sigma_g^+$ states

Figure 6 presents two $v=1$ $g\ ^3\Sigma_g^+$ state spectra and the corresponding expansion coefficients $f_k(R)$. The figures on the left-hand side correspond to a low branching ratio, $N=1$. The most important contributions to this nonadiabatic state are from the $3d\ ^3\Sigma_g^+$ (dashed) and $i\ ^3\Pi_g$ (dash-dotted) electronic states. The electronic $j\ ^3\Delta_g$ state contribution vanishes since it offers no $N=1$ rotational level. On increasing angular momentum (the figures on the right-hand side correspond to $N=5$), the electronic $i\ ^3\Pi_g$ state contribution increases at the expense of the $3d$

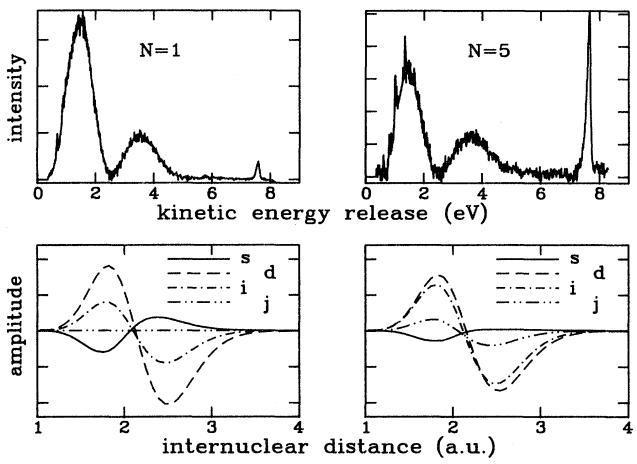

FIG. 6. Plots of $v=1$ $g\,^3\Sigma_g^+$ state KER spectra for different angular-momentum values, and, under each of them, correspondingly, the computed expansion coefficients $f_i(R)$ of Eq. (3) that illustrate the electronic mixing. The broad structure extending from 0 to 5 eV arises from fragmentation following fluorescence to the dissociative $b\,^3\Sigma_u^+$ state; the peak near 7.5 eV arises from fragmentation following fluorescence to the rapidly predissociated $c\,^3\Pi_u^+$ state.

$^3\Sigma_g^+$ state contribution. From the corresponding transition dipole moments [Figs. 4(a) and 4(b)] one can appreciate that a pure $i\,^3\Pi_g$ state has a larger branching ratio than a pure $3d\,^3\Sigma_g^+$ state. The electronic $j\,^3\Delta_g$ state contribution also tends to increase the branching ratio: Since the $j\,^3\Delta_g$ to $b\,^3\Sigma_u^+$ state transition is electric dipole forbidden, a pure $j\,^3\Delta_g$ state has an infinite branching ratio. Thus the increased electronic $i\,^3\Pi_g$ and $j\,^3\Delta_g$ state contributions explain the observed increased fluorescence to the $c\,^3\Pi_u^+$ state. A similar argument applies to the opposite branching behavior of the $h\,^3\Sigma_g^+$ state, which decreases with increasing angular momentum. For increasing N the $h\,^3\Sigma_g^+$ state has a decreasing electronic $i\,^3\Pi_g$ state contribution to the benefit of the $3s\,^3\Sigma_g^+$ state contribution. Again a pure $i\,^3\Pi_g$ state has a larger branching ratio than a pure $3s\,^3\Sigma_g^+$ state, as can be seen from the transition dipole moments, and the experimentally observed branching-ratio behavior is confirmed.

$N=0$ branching ratios do not fit the trends set by levels with higher angular momenta. This anomaly reflects the impossibility of an $N=0$ nonadiabatic $^3\Sigma_g^+$ state mixing with available Π and Δ states, in contrast to the $^3\Sigma_g^+$ states with higher angular momentum N.

Unfortunately the metastable beam composition, consisting of the negative-parity $c\,^3\Pi_u^-$ state component only, does not allow for excitation of positive-parity $N=0$ rotational levels. This prevents us from demonstrating experimentally this example of discontinuous behavior in molecular processes.

2. $i\,^3\Pi_g$ and $j\,^3\Delta_g$ states

The $j\,^3\Delta_g$ state branching behavior is readily understood. Due to its Δ symmetry a pure $j\,^3\Delta_g$ state cannot radiate to the $b\,^3\Sigma_u^+$ state since this is an electric-dipole-forbidden transition ($\Delta\Lambda=2$). Hence, a pure $j\,^3\Delta_g$ state yields an infinite branching ratio. The branching ratios for the nonadiabatic $j\,^3\Delta_g^{\pm}$ states, though large, are not infinite and represent a direct measure for mixing of mainly the electronic $i\,^3\Pi_g$ state.

The nonadiabatic $i\,^3\Pi_g^-$ states show a minimum in their branching ratios at about $N=3$. This minimum is a consequence of two factors with opposite behavior: for increasing angular momentum, increasing electronic $j\,^3\Delta_g$ state admixture leads to increasing branching ratios, while the ratio of rotational wave-function overlap, given by the $3j$ symbol in Eq. (4), leads to decreasing branching ratios. An anomaly in the calculated branching ratios for $N=1$ can be seen that is similar to the $N=0$ $^3\Sigma_g^+$ states described above, since the $N=1$ $i\,^3\Pi_g^-$ state is pure, in contrast to the higher angular-momentum levels, which can mix with the electronic $j\,^3\Delta_g$ state. For the positive-parity nonadiabatic $i\,^3\Pi_g^+$ state the situation is more complicated due to additional $^3\Sigma_g^+$ state admixture, and qualitative explanation of the branching-ratio behavior as done above is not possible.

V. CONCLUSION

In a previous report from this laboratory Koot *et al.* also presented a number of branching ratios [3]. Better detection calibration and signal-to-noise ratios have enabled us to improve on the branching-ratio accuracy. However, the main achievement of this work is the detailed understanding of the branching-ratio behavior in terms of the electronic composition of the total, nonadiabatic wave function. A detailed description of the mixing of electronic states in the nonadiabatic state has been presented before by Keiding and Bjerre [9] and Alikacem and Larzillière [10]. By means of a model Hamiltonian line fit that takes into account L uncoupling, both groups were able to obtain considerable insight into the rotational perturbations affecting the $n=3$ triplet gerade complex in HD and H_2, respectively. The present experiments also provide an exact understanding of vibrational coupling between the electronic $^3\Sigma_g^+$ states, which cannot be offered by the L-uncoupling model Hamiltonian treatment. The combination of rotational and vibrational mixing leads to a complicated nonadiabatic state composition. This composition is directly reflected in the behavior of the branching ratios and in the shape of the KER spectra for emission to the $b\,^3\Sigma_u^+$ state. Agreement of theory with the present experimental data constitutes important evidence for the reliability of the vibrational couplings calculated in paper I.

ACKNOWLEDGMENTS

This work is part of the research program of the Stichting voor Fundamenteel Onderzoek der Materie (Foundation for Fundamental Research on Matter) and was made possible by financial support of the Nederlandse Organisatie voor Wetenschappelijk Onderzoek (Organization for Scientific Research). It was partly performed under auspices of the Office of Basic Energy Sciences, Division of Chemical Sciences, U.S. Department of Energy under Contract No. W-31-109-ENG-38.

[1] J. M. Schins, L. D. A. Siebbeles, W. J. van der Zande, and J. Los, preceding paper, Phys. Rev. A **44**, 4162 (1991).

[2] P. Senn, P. Quadrelli, and K. Dressler, J. Chem. Phys. **89**, 7401 (1988).

[3] W. Koot, W. J. van der Zande, P. H. P. Post, and J. Los, J. Chem. Phys. **90**, 4826 (1989); W. Koot, P. H. P. Post, W. J. van der Zande, and J. Los, Z. Phys. D **10**, 233 (1988).

[4] D. P. de Bruijn and H. Helm, Phys. Rev. A **34**, 3855 (1986); H. Helm, D. P. de Bruijn, and J. Los, Phys. Rev. Lett. **53**, 1642 (1984).

[5] D. P. de Bruijn and J. Los, Rev. Sci. Instrum. **53**, 1020 (1982).

[6] L. D. A. Siebbeles, J. M. Schins, J. Los, and M. Glass-Maujean, Phys. Rev. A **44**, 1584 (1991).

[7] Since we deal with positive-parity final states exclusively, the selection rules imply P and R branches from initial positive-parity states, and a Q branch from initial negative-parity states.

[8] J. M. Schins, L. D. A. Siebbeles, W. J. van der Zande, and J. Los, Chem. Phys. Lett. **182**, 69 (1991).

[9] S. R. Keiding and N. Bjerre, J. Chem. Phys. **87**, 3321 (1990).

[10] A. Alikacem and M. Larzillière, J. Chem. Phys. **93**, 215 (1990).

[11] J. Rychlewski (unpublished results). The transition dipole moments for the h-b, g-b, h-c, and g-c transitions were calculated using explicitly correlated wave functions containing 130, 135, 110, and 75 terms for the $h\ ^3\Sigma_g^+$, $g\ ^3\Sigma_g^+$, $b\ ^3\Sigma_u^+$, and $c\ ^3\Pi_u$ states, respectively.

[12] J. M. Schins, L. D. A. Siebbeles, J. Los, M. Kristensen, and H. Koch, J. Chem. Phys. **93**, 3887 (1990).

[13] R. J. Harrison and S. Zarrabian, Chem. Phys. Lett. **158**, 393 (1989); H. Koch and R. J. Harrison, J. Chem. Phys. (to be published).